Chem. Pap. (2017) 71:579–595
DOI 10.1007/s11696-016-0040-4

ORIGINAL PAPER

Controlled synthesis of graphene oxide/alumina nanocomposites using a new dry sol–gel method of synthesis

Agnieszka Maria Jastrzębska[1] · Joanna Jureczko[2] · Joanna Karcz[1] · Antoni Kunicki[2] · Wanda Ziemkowska[2] · Andrzej Olszyna[1]

Received: 11 March 2016 / Accepted: 22 August 2016 / Published online: 14 December 2016

Abstract The present paper gives new insight into the problem of controlling the morphology of reduced graphene oxide/alumina (RGO/Al_2O_3) nanocomposites. The dry and simplified sol–gel methods of RGO/Al_2O_3 nanocomposite synthesis were compared and the influence of six key synthesis parameters on the morphology of the resulting nanocomposite powders was investigated to optimize the morphology of RGO/Al_2O_3 nanocomposites in terms of reducing the undesired agglomeration of RGO/Al_2O_3 nanocomposite flakes to a significant minority and obtaining the uniform coverage of RGO surface with Al_2O_3 nanoparticles. Our investigations indicate that, despite the high excess of Al_2O_3 used (95 wt%), the lowest RGO/Al_2O_3 flake agglomeration and the formation of a uniform layer composed of Al_2O_3 nanoparticles with the average size of 58 nm occurred only when 5 wt% of graphene oxide was used as a substrate for the deposition of Al_2O_3 nanoparticles together with triethyl aluminium as an Al_2O_3 precursor and dry hexane as the reaction environment. The resulting organic precursor was thermally decomposed at 280 °C for 3 h in air atmosphere (R4 reaction pathway). This was confirmed by the high BET-specific surface area (242.4 m^2/g) and the high open porosity (0.7 cm^3/g) of the obtained RGO(5 wt%)/Al_2O_3 nanocomposite. This is also the first study with a detailed discussion of the reactions expected to occur during the synthesis of an RGO/Al_2O_3 nanocomposite.

Keywords Graphene nanocomposites · Graphene oxide · Aluminium oxide · Nanoparticles · Synthesis optimization · Sol–gel reactions

Introduction

The pioneering study of graphene by Geim and Novoselov (Novoselov et al. 2004) made the world aware of a new member of carbon nanostructures. Since then, many interesting functional properties have been described (Neto et al. 2009; Zhang et al. 2011) together with unique bioactivity (Jastrzębska et al. 2012), drawing scientific attention and technological interest to graphene. Lately, it has been shown that graphene and its related materials show great promise for potential applications in, e.g. biosensors, adsorbents for heavy metal removal (Zhang et al. 2011), as well as lithium ion batteries and electrochemical supercapacitors (Li et al. 2011). It has also been shown that, by deposition of different nanoparticles on graphene sheets, it is possible to develop composite materials and, as a result, improve the properties of the deposited nanoparticles by utilizing the specific electrical properties of graphene (Jiang et al. 2011; Liang et al. 2010; Peter et al. 2015). It is also known that the modification of graphene oxide (GO) during in situ methods is realized mainly through covalent bonding between nanoparticle precursors and oxygen-containing functional groups that are known to exist on GO surface resulting in reduction to reduced graphene oxide (RGO) (Liang et al. 2010; Wang et al. 2010; Jastrzębska et al. 2015, 2016). The possibility of nanoparticle detachment from graphene surface is

✉ Agnieszka Maria Jastrzębska
agsolgala@gmail.com

[1] Faculty of Materials Science and Engineering, Warsaw University of Technology, Wołoska 141, 02-507 Warsaw, Poland

[2] Faculty of Chemistry, Warsaw University of Technology, Noakowskiego 3, 00-664 Warsaw, Poland

highly valuable (Singh et al. 2011). It is also accepted that the so-called wet sol–gel methods can be used for in situ GO modification techniques, e.g. the preparation of solid RGO/SiO_2 thin films for transparent conductors (Watcharotone et al. 2007) as well as solid layers of RGO/Al_2O_3 for catalytic hydrodesulfurization (Tian et al. 2015). The latter method consists of the wet hydrolysis of boehmite in acidic environment and subsequent thermal treatment. The recent findings of Ziemkowska and co-workers (Ziemkowska et al. 2014) also indicate that the morphology of Al_2O_3 nanopowder synthesized using a wet sol–gel method is strictly dependent on the amount of water introduced to the reaction environment and that the lack of H_2O results in obtaining agglomerates or sponge-like structures. Recently, a new dry sol–gel method for the synthesis of RGO(5 wt%)/Al_2O_3 nanocomposites has been investigated (Jastrzębska et al. 2015). The method was realized in a full-dry environment (no hydrolysis or condensation during the reaction), in contrast to conventional wet sol–gel methods (in which water is introduced to the reaction). The main disadvantage was that the Al_2O_3 nanoparticles often agglomerated on the surface of RGO flakes resulting in the undesirable aggregation of some part of the final product (not uniform, porous and agglomerated layer of Al_2O_3). Lately, a simplified sol–gel method has been analysed for the production of an RGO/Al_2O_3 (40 wt%) nanocomposite (Jastrzębska et al. 2016). The method was expected to be simplified relative to the dry sol–gel method. Mild hydrolysis and condensation were not separated as a single stage but were initiated at the start of the process as a result of H_2O present in the air and occurred during the whole progress of the process. Aluminium triisopropoxide was used as an Al_2O_3 precursor, and dry isopropanol was the reaction environment. However, the agglomeration of Al_2O_3 nanoparticles on the edges and flexures of RGO was still observed. Al_2O_3 nanoparticles were distributed on the surface of GO flakes non-homogenously, and the measured average particle size was more than three times higher in comparison with free Al_2O_3 nanoparticles (Jastrzębska et al. 2016). The present paper gives new insight into the problem of controlling and optimizing the morphology of RGO/Al_2O_3 nanocomposites. The dry and simplified sol–gel methods for the synthesis of RGO/Al_2O_3 nanocomposites were also compared, and the influence of six key synthesis parameters on the morphology of the resulting nanocomposite powders was investigated to reduce the undesired agglomeration of the nanocomposite flakes to a significant minority. This is also the first study with a detailed discussion of the reactions expected to occur during the synthesis of an RGO/Al_2O_3 nanocomposite together with the proposed reaction sequences.

Experimental

Reduction of GO to RGO

In the present study, we used commercial GO flakes (Cheap Tubes Inc., USA) and we prepared RGO flakes by ourselves. The vacuum-assisted thermal reduction process was used for the reduction of GO to RGO. It is accepted that thermal reduction is a simple and clean way to almost completely remove oxide-containing functional groups from GO surfaces by utilizing vacuum-assisted heat treatment (Erickson et al. 2010; Mavarro et al. 2010; Yang et al. 2009a; Mattevi et al. 2009). Our results show that the thermal treatment of GO flakes at 150 °C in a 3×10^{-2} Torr vacuum for a period of 6 h resulted in a change of the colour of GO from brown to black. The GO and RGO flakes were further used in the reaction processes.

Different parameters of RGO/Al_2O_3 nanocomposite synthesis

It is known that hydrophobic/hydrophilic incompatibility between graphene and metal oxide nanoparticles makes their deposition highly difficult (Wang et al. 2008). Conversely, GO is also widely known as a good candidate for supporting metal or metal oxide nanoparticles due to the presence of reactive oxygen-containing species on its surface (C–OH, O=C–OH, C=O, or C_2O). In this study, the compatibility between RGO and Al_2O_3 nanoparticles is addressed in detail in parallel to the optimized method of its synthesis. The considered synthesis processes leading to different RGO/Al_2O_3 nanocomposite powders with different morphologies are presented in Fig. 1. As can be seen, the influence of six key synthesis parameters on the morphology of resulting RGO/Al_2O_3 nanocomposite powders was investigated. The analysis took into account parameters such as:

1. the type of aluminium oxide organic precursor (triethylaluminium, Et_3Al, or aluminium triisopropoxide, Al(*i*-PrO)$_3$);
2. the type of reaction environment (hexane or isopropanol (*i*-PrOH));
3. the type of graphene used as a substrate for the deposition of Al_2O_3 nanoparticles (GO or RGO);
4. the thermal annealing temperature (280 or 500 °C);
5. the concentration of RGO(0, 5, 10, or 15 wt%) in the final product;
6. the concentration of the modifier, diethyl ether (Et_2O) (1 or 3 wt%).

The procedures of sol–gel synthesis of RGO/Al_2O_3 nanocomposites were as follows:

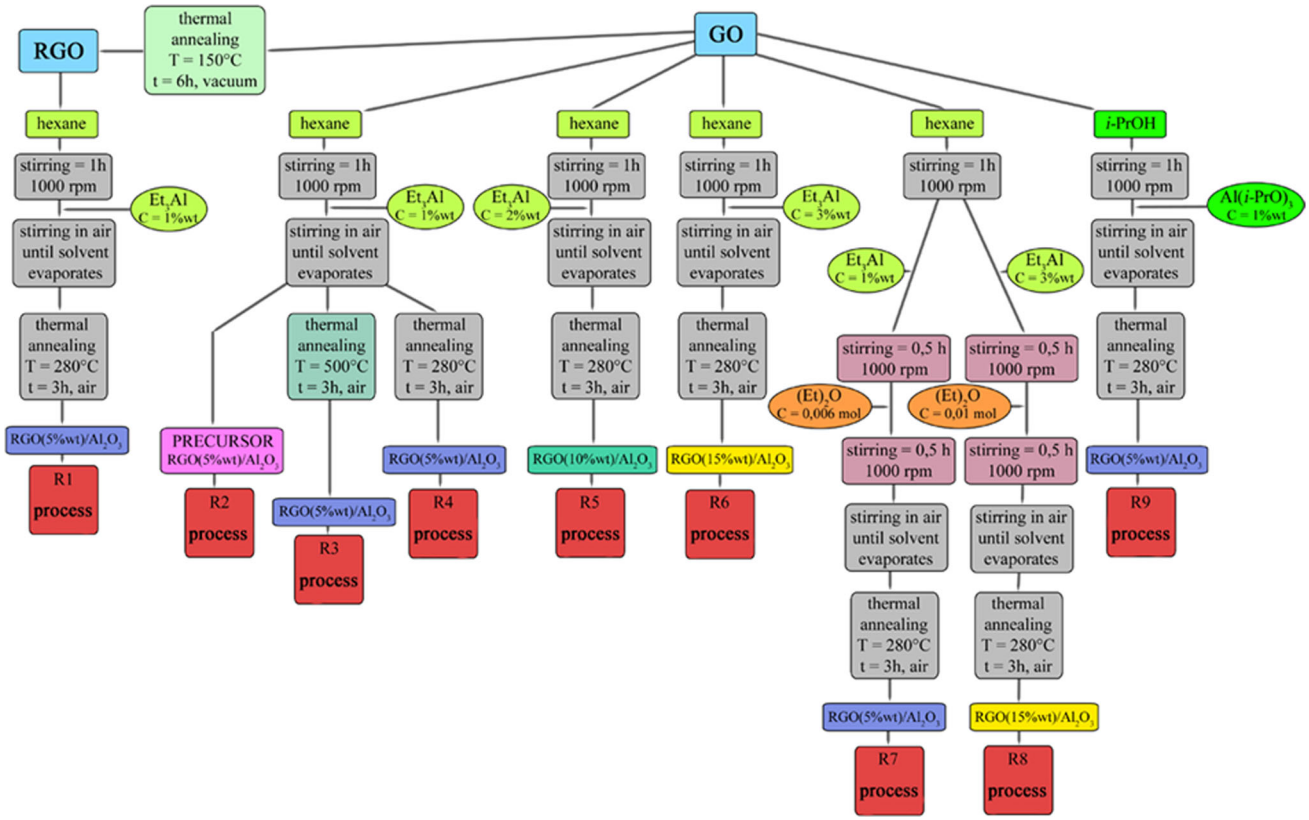

Fig. 1 Flowchart presenting different procedures of RGO/Al_2O_3 nanocomposite synthesis considered for the analysis of the influence of key synthesis parameters on the composite morphology

For the R1 process, 500 ml of dry hexane was introduced to a 1000 ml reactor equipped with a magnetic stirrer. Then, 0.01 g of RGO flakes was added to the hexane, and the resulting suspension was stirred for 1 h at 1000 rpm. Subsequently, 0.5 ml of 1 wt% solution of trimethylaluminium was introduced, and the reaction mixture was stirred in air until the spontaneous evaporation of the solvent. After that, the dark brown powder of the intermediate product (organic precursor) was obtained. After the thermal decomposition of the precursor (280 °C, 3 h, air atmosphere) in a muffle furnace, the black final product of the RGO(5 wt%)/Al_2O_3 nanocomposite was obtained.

For the R2-4 processes 500 ml of dry hexane was introduced to a 1000 ml reactor equipped with a magnetic stirrer. Then, 0.1 g of GO flakes was added to the hexane, and the resulting suspension was subsequently stirred for 1 h at 1000 rpm. Subsequently, 0.5 ml of 1 wt% solution of trimethylaluminium was introduced, and the reaction mixture was stirred in air until the spontaneous evaporation of the solvent. After that, the dark brown powder of the intermediate product (organic precursor) was obtained. The sample of the organic precursor was divided into three parts. The first part of the sample was directly subjected to SEM analysis (see the R2 process). The second part of the sample was subjected to thermal decomposition at 500 °C for 3 h in air atmosphere in a muffle furnace (see the R3 process), whereas the third part of the sample was thermally decomposed at 280 °C for 3 h in air atmosphere (see the R4 process). After thermal annealing, the black final products of the RGO(5 wt%)/Al_2O_3 nanocomposites were obtained.

For the R5 and R6 processes 500 ml of dry hexane was introduced to a 1000 ml reactor equipped with a magnetic stirrer. Then, 0.01 g of GO flakes was added to the hexane, and the resulting suspension was subsequently stirred for 1 h at 1000 rpm. The reaction mixture was divided into two parts, and 1 and 1.5 ml of 2 or 3 wt% solution of trimethylaluminium was introduced for the R5 and the R6 processes, respectively. Then, the reaction mixtures were stirred in air until the spontaneous evaporation of the solvent. After that, the dark brown powder of the intermediate products (organic precursors) was obtained. After thermal annealing at 280 °C for 3 h in air atmosphere, the black final products of the RGO(10 wt%)/Al_2O_3 and RGO(15 wt%)/Al_2O_3 nanocomposites were obtained for the R5 and R6 processes, respectively.

For the R7 and R8 processes 500 ml of dry hexane was introduced to a 1000 ml reactor equipped with a magnetic stirrer. Then, 0.01 g of GO flakes was added to the hexane, and the resulting suspension was subsequently stirred for 1 h at 1000 rpm. The reaction mixture was divided into two parts, and 0.5 and 1.5 ml of 1 or 3 wt% solution of trimethylaluminium was introduced for the R7 and the R8 processes, respectively. Then, the reaction mixtures were stirred for 0.5 h at 1000 rpm. After that time, 0.003 ml and 0.01 ml of 8.65×10^{-5} or 2.58×10^{-5} mol of $(Et)_2O$ was added for the R7 and R8 processes, respectively. Subsequently, the reaction mixtures were stirred for 0.5 h at 1000 rpm. After that time, the reaction mixtures were stirred in air until the spontaneous evaporation of the solvent. The dark brown powder of the intermediate products (organic precursors) was obtained. After thermal annealing at 280 °C for 3 h in air atmosphere, the black final products of the RGO(5 wt%)/Al_2O_3 and RGO(15 wt%)/Al_2O_3 nanocomposites were obtained for the R7 and R8 processes, respectively.

For the R9 process 500 ml of dry isopropyl alcohol was introduced to a 1000 ml reactor equipped with a magnetic stirrer. Then, 0.01 g of GO flakes was added to the isopropyl alcohol, and the resulting suspension was subsequently stirred for 1 h at 1000 rpm. Then, 0.02 g of aluminium triisopropoxide was introduced. After that, the reaction mixture was stirred in air until the spontaneous evaporation of the solvent, and the dark brown powder of the intermediate product (organic precursor) was obtained. After thermal annealing at 280 °C for 3 h in air atmosphere, the black final product of the RGO(5 wt%)/Al_2O_3 nanocomposite was obtained.

For the synthesis of Al_2O_3 nanopowder, we used a process similar to the one presented for the R4 process, excluding the stage of GO addition.

Chemicals and substrates used

Chemicals used in the RGO/Al_2O_3 nanocomposite synthesis (hexane, isopropyl alcohol, triethylaluminium, aluminium triisopropoxide, diethyl ether) were purchased from Sigma-Aldrich (Gillingham, Dorset, UK). Trimethylaluminium was moisture sensitive, and it was stored under argon atmosphere. GO flakes were purchased from Cheap Tubes Inc. (USA) and were synthesized from natural graphite powders by a modified Hummer's method, which uses a combination of potassium permanganate and sulphuric acid.

Investigation methodology

The GO flakes, RGO flakes, RGO/Al_2O_3 nanocomposites, and Al_2O_3 nanopowder were examined in terms of the obtained morphology and physical properties. The methodology used for the characterization of the obtained materials was similar to that described in our previous publications (Jastrzębska et al. 2015, 2016). Briefly, a scanning electron microscope (SEM-LEO 1530, Zeiss, USA) was used for morphology observations. Samples were deposited onto the surface of a carbon tape and coated with a thin carbon layer The elemental EDS analysis was used for the analysis of the local contents of the elements present in a given region for the chosen RGO/Al_2O_3 nanocomposite. The obtained SEM images were subsequently analysed quantitatively using statistical (stereological) analysis and the MicroMeter v.086b computer program. The analysis took into account the mean value E(x) and the coefficient of variation CV(x) of the stereological parameters such as the equivalent diameter d_2; the maximum value of the chord of particle d_{max}; the minimum value of the chord of particle d_{min}; the particle perimeter p; the Couchi perimeter pC, as well as the particular coefficients of shape: d_{max}/d_2, d_{min}/d_2, $p/\pi d_2$, and p/pC. The additional parameter n represents the number of measured values.

The isotherms of physical nitrogen sorption $V = f(p/p^\circ)$ were measured experimentally, using a Quadrasorb-SI device (Quantachrome Instruments, USA) at a temperature of −195.8 °C, within the entire range of the relative pressure. The specific surface area, S_{BET}, was determined using the Brunauer, Emmett, Teller (BET) method and the total volume of the pores, V_{BJH}, present in the samples was determined using the Barret, Joyner, Halenda (BJH) method. The distributions of pore sizes were further used for the estimation of the average pore size, D_{BJH}.

The quantitative chemical composition of the RGO/Al_2O_3 nanocomposite was also analysed using the XPS spectroscopy (Microlab 350 spectrometer from Thermo Electron) with soft X-Ray radiation as the source of excitation (AlK_α radiation, $h\nu = 1486.6$ eV; Al; 200 W). The peak of C1s = 285.0 eV (binding of CC/CH) was used as the internal standard.

Results and discussion

Recently, we have published the preliminary investigations results on a new dry sol–gel method (Jastrzębska et al. 2015) and a simplified sol–gel method (Jastrzębska et al. 2016) of the synthesis of well-dispersible RGO/Al_2O_3 nanocomposites. To obtain RGO flakes, the vacuum-assisted thermal reduction process was used in the present study for the reduction of GO. It is known that to obtain RGO two possible chemical routes can be applied in particular: methods where a solvent is used (wet methods) and the so-called dry methods. Numerous literature data have

been published on the wet chemical reduction of GO sheets. It can be performed with several reducing agents, e.g. hydrazine (Becerril et al. 2008), sodium borohydrate (Shin et al. 2009), hydroquinone (Wang et al. 2008), or even strongly alkaline solutions (Fan et al. 2008). During the reduction process, the brown-coloured dispersion of GO in the solvent turns black and the reduced sheets aggregate and precipitate (Stankovich et al. 2007). Dry reduction methods are, however, cleaner than wet ones and can be performed using, e.g. gaseous hydrogen (after thermal expansion) (Wu et al. 2009). Thermal reduction is a simple and clean way to reduce GO and utilizes heat treatment to remove the oxide functional groups from GO surfaces. Different heat treatments have been used so far at different final temperatures (200, 500, and 1000 °C) in argon atmosphere or ultrahigh vacuum (10^{-8} Torr) to study the possible reduction of films composed of GO (Yang et al. 2009b). A significant reduction of GO has been observed, resulting in the complete disappearance of C=O and O=C–OH species with the exception of C–OH. The authors have suggested that, even after the 1000 °C treatment of GO, the remaining C–OH groups are still present because their reduction is very difficult from the thermodynamical point of view. Other authors' results also confirm this assumption (Erickson et al. 2010; Mavarro et al. 2010). It is accepted that even ultrahigh vacuum assistance (Mattevi et al. 2009) is not sufficient to completely remove all of the oxygen from the GO surface. Our observations showed that the heat treatment of GO flakes at 150 °C in vacuum for a period of 6 h resulted in the colour of GO changing from brown to black.

Morphology

The morphology of GO flakes and RGO flakes (used as substrates for Al_2O_3 nanoparticle deposition) was examined qualitatively using a scanning electron microscope (SEM). Figure 2 shows the morphology of the analysed GO and RGO samples. It can be seen that both GO and RGO flakes possessed an irregular shape which can be described as 'curly' (Fig. 2a, b, respectively). Our results indicate that thermal annealing made it possible to obtain a similar morphology of the resulting RGO flakes in comparison with GO. Also, the high magnification views show the smooth surfaces of GO and RGO flakes. Their lateral dimensions were ca. 4 μm.

The influence of six key synthesis parameters on the morphology of the resulting RGO/Al_2O_3 nanocomposite powders was investigated qualitatively using an SEM. The analysis took into account parameters, such as: (1) type of aluminium oxide organic precursor (trimethylaluminium, Et_3Al, or aluminium triisopropoxide, Al(*i*-PrO)$_3$); (2) type of reaction environment (hexane or isopropanol (*i*-PrOH)), (3) type of graphene used as a substrate for the deposition of Al_2O_3 nanoparticles (GO or RGO), (4) thermal annealing temperature (280 or 500 °C), (5) concentration of RGO(0, 5, 10, or 15 wt%) in the final product, and (6) concentration of the modifier, Et_2O (1 or 3 wt%). The obtained investigation results showed that the above-mentioned factors have a major influence on the morphology of the investigated RGO/Al_2O_3 nanocomposites.

The morphologies of RGO(5 wt%)/Al_2O_3 nanocomposites obtained in the R4 and R9 processes are presented in Fig. 3a, b, respectively. The obtained nanocomposites differed only in the type of aluminium oxide organic precursor used in the synthesis process. Trimethylaluminium (Et_3Al) was used as the Al_2O_3 organic precursor in the R4 process, whereas aluminium triisopropoxide (Al(*i*-PrO)$_3$) was used in the R9 process. It can be seen that the RGO(5 wt%)/Al_2O_3 nanocomposite obtained by the R4 process was characterized by less agglomeration in comparison with the nanocomposite obtained in the R9 process. The Al_2O_3 nanoparticles deposited on the surface of RGO flakes (Fig. 3a) were much easier to identify and, as can be seen in the high magnification image, acted as a spreader between individual RGO flakes. The agglomeration of the RGO(5 wt%)/Al_2O_3 nanocomposite obtained by the R9 process (Fig. 3b) was so high that not even a single RGO flake was able to be identified. It should also be noted that hexane was used as the reaction environment in the R4 process, whereas isopropanol (*i*-PrOH) was used in the R9 process. As can be seen, the best morphology in the case of the RGO(5 wt%)/Al_2O_3 nanocomposite was obtained when trimethylaluminium was used as an Al_2O_3 nanoparticle organic precursor together with hexane as the reaction environment.

The morphologies of RGO(5 wt%)/Al_2O_3 nanocomposites obtained in the R4 and R1 processes are presented in Fig. 4a, c, respectively. The obtained nanocomposites differed in the type of graphene used as the substrate for the deposition of Al_2O_3 nanoparticles. In the R4 process, GO was used as the substrate, whereas in the R1 process, RGO was used. As can be seen on SEM images, GO was a better choice for a substrate. RGO(5 wt%)/Al_2O_3 nanocomposites obtained using RGO were characterized by higher agglomeration.

The morphologies of RGO(5 wt%)/Al_2O_3 nanocomposites obtained in the R2, R4, and R3 processes are presented in Fig. 4a–c, respectively. The obtained nanocomposites differed in the temperature of thermal annealing used in the synthesis process. The powder obtained in the R2 process (RGO/Al_2O_3 organic precursor) was subjected to SEM observations without any thermal treatment, directly after the evaporation of the solvent. The RGO(5 wt%)/Al_2O_3 nanocomposite obtained in the R4 process was thermally decomposed at 280 °C, whereas 500 °C was used in the R3

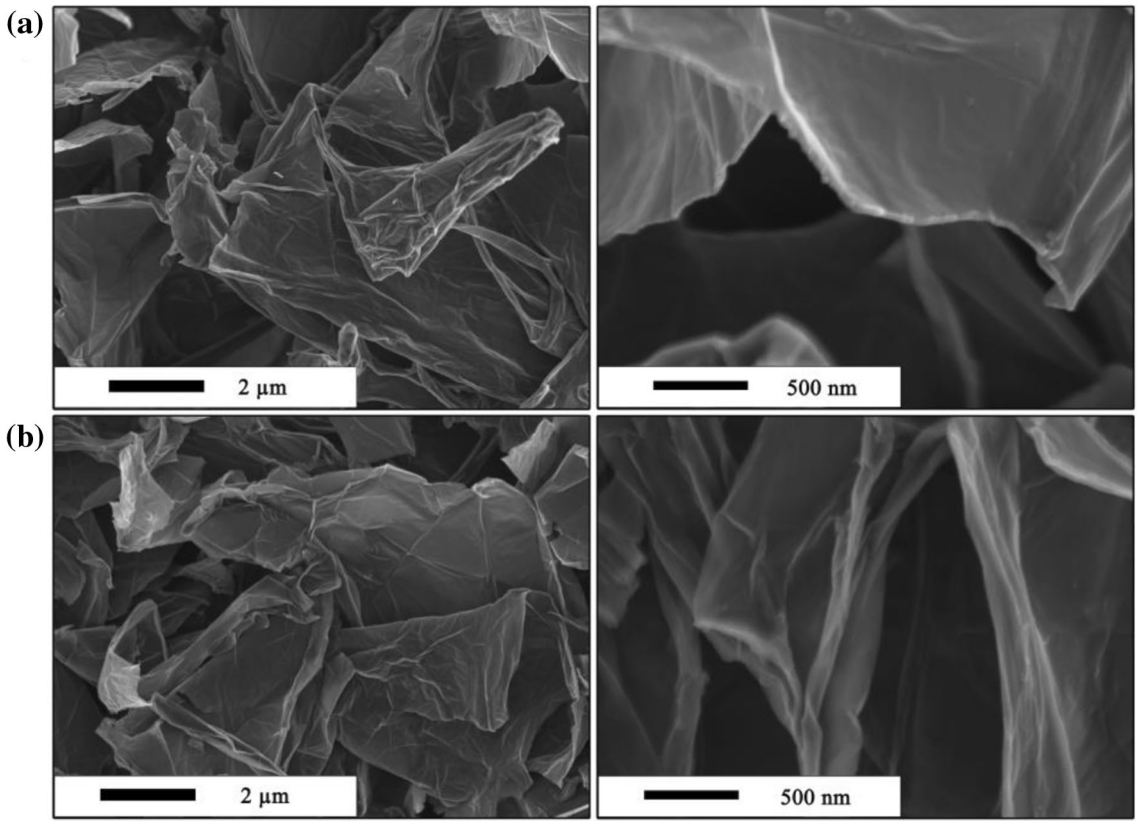

Fig. 2 SEM images obtained for **a** the GO and **b** the RGO flakes

process for the thermal decomposition of the organic precursor. The investigation results indicate that the process of thermal treatment has a significant influence on the morphology of the final product. The RGO(5 wt%)/Al_2O_3 nanocomposite thermally treated at 500 °C was much more agglomerated than the one treated at 280 °C. As can be seen in Fig. 4, thermal treatment generally stimulates the growth and agglomeration of Al_2O_3 nanoparticles deposited on the edges of RGO flakes. When considering the organic precursor, it can be seen that the number of Al_2O_3 agglomerates attached to the edges of RGO flakes was a minority and also a majority in RGO(5 wt%)/Al_2O_3 nanocomposite thermally treated at 500 °C. This indicates that the temperature chosen for the thermal decomposition of the nanocomposite organic precursor should be far below 500 °C. Thus, the temperature of 280 °C should be considered optimal for the decomposition of aluminium triethoxide and the formation of Al_2O_3 nanoparticles characterized most probably by a low-temperature (amorphous) phase of alumina.

The morphologies of RGO/Al_2O_3 nanocomposites with 0, 5, 10, and 15 wt% of Al_2O_3 addition are presented in Fig. 5. The above-mentioned concentrations of Al_2O_3 in the final product correspond to the each of the particular reaction processes, such as: R4 (Al_2O_3), R4, R5, and R6, respectively. For the synthesis of the Al_2O_3 nanopowder, we used a similar process to that described for R4, excluding the stage of GO addition. The morphology of the Al_2O_3 nanopowder is presented in Fig. 5a. As can be seen, it is composed of agglomerates and single nanoparticles of sizes not exceeding 200 nm. This morphology can be described as typical for Al_2O_3 nanopowders obtained by us previously in sol–gel processes (Jastrzebska et al. 2011a, b; c, 2013, 2014, 2015b; Ziemkowska et al. 2014; Polis et al. 2013; Jusza et al. 2011, Karwowska et al. 2002). In the R4 process, the 5 wt% addition of RGO flakes to the nanocomposite results in less agglomeration of the final product as a result of the deposition of Al_2O_3 nanoparticles on the surface of RGO flakes (Fig. 5b). The rest of the alumina organic precursor, not utilized on the surface of the flakes, existed as agglomerates composed mainly of Al_2O_3 nanoparticles. As can be seen, the reduction of Al_2O_3 sizes when deposited on RGO was achieved. It should be mentioned that in our previous investigation results the average particle size of Al_2O_3 deposited on RGO was more than three times higher in comparison with free Al_2O_3 nanoparticles (Jastrzębska et al. 2016). It is expected that an increase of the RGO addition should decrease the presence of free Al_2O_3 agglomerates. This was, however, not confirmed with the RGO/Al_2O_3

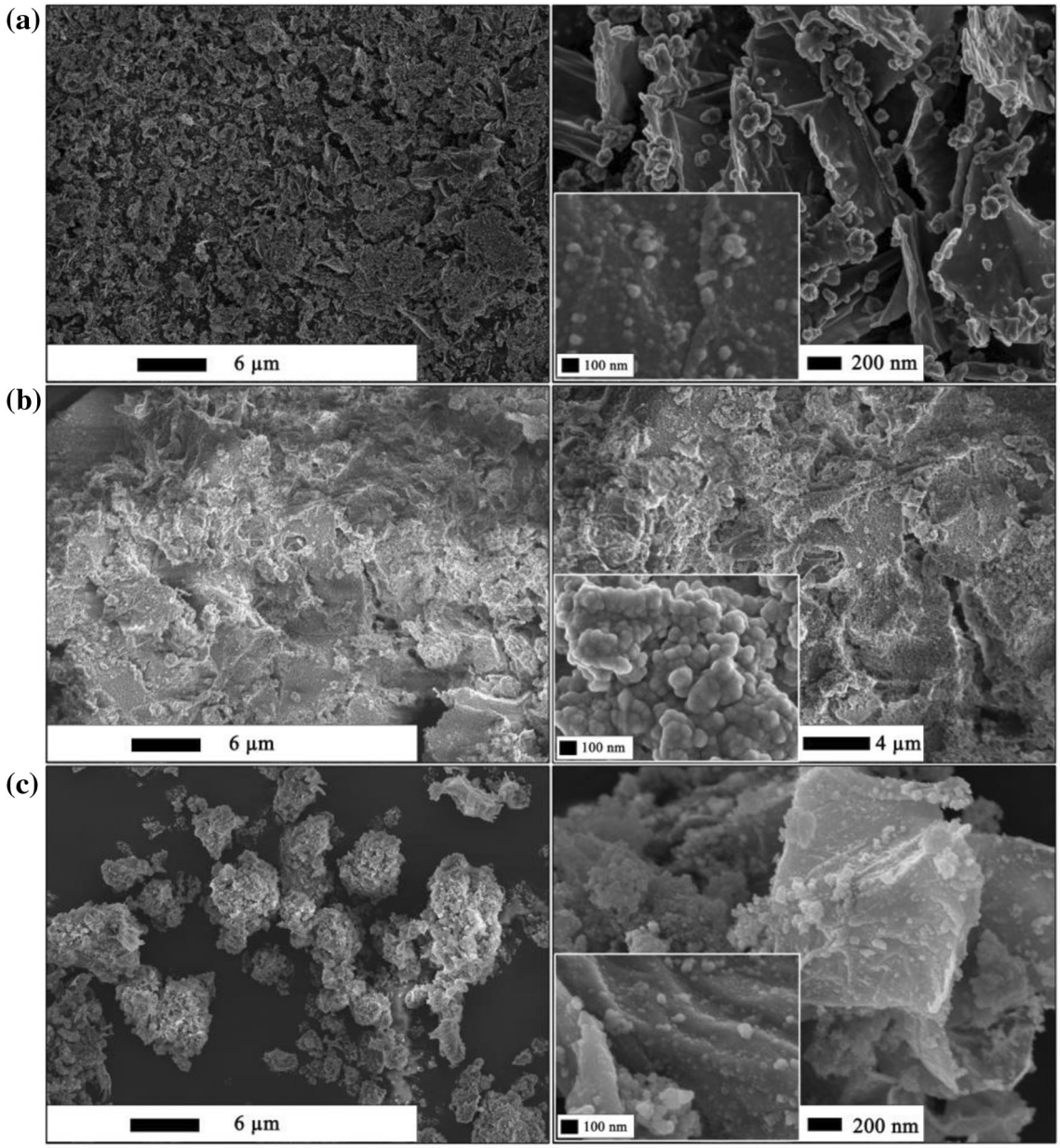

Fig. 3 SEM images obtained for the RGO(5 wt%)/Al_2O_3 nanocomposites obtained in **a** the R4, **b** the R9, and **c** the R1 process

(10 wt%) sample because of final product agglomeration (Fig. 5c). On the other hand, when considering the nanocomposite with 15 wt% addition of RGO flakes (Fig. 5d), it can be seen that the number of free Al_2O_3 agglomerates highly decreased in comparison with the rest of the samples. As can be seen, however, on a high magnification image, some of the GO flakes were not covered with Al_2O_3 nanoparticles.

The morphologies of RGO(5 wt%)/Al_2O_3 nanocomposites obtained in the R4 and R7 processes are presented in Fig. 6. The nanocomposite obtained in the R7 process was modified with 0.006 ml of Et_2O. As compared with the RGO(5 wt%)/Al_2O_3 nanocomposite non-modified with Et_2O (Fig. 5a), the above-mentioned modification resulted in the higher agglomeration of the final product and the formation of a high amount of Al_2O_3 agglomerates attached to the edges and the surface of RGO flakes (Fig. 6b).

The morphologies of RGO(15 wt%)/Al_2O_3 nanocomposites obtained in the R6 and R8 processes are presented in Fig. 7. The nanocomposite obtained in the R8 process was modified with 0.01 ml of Et_2O. As compared with the RGO(15 wt%)/Al_2O_3 nanocomposite non-modified with Et_2O (Fig. 7a), the above-mentioned modification resulted in improvement in covering the surface of RGO flakes (Fig. 7b). This can be clearly seen in the high

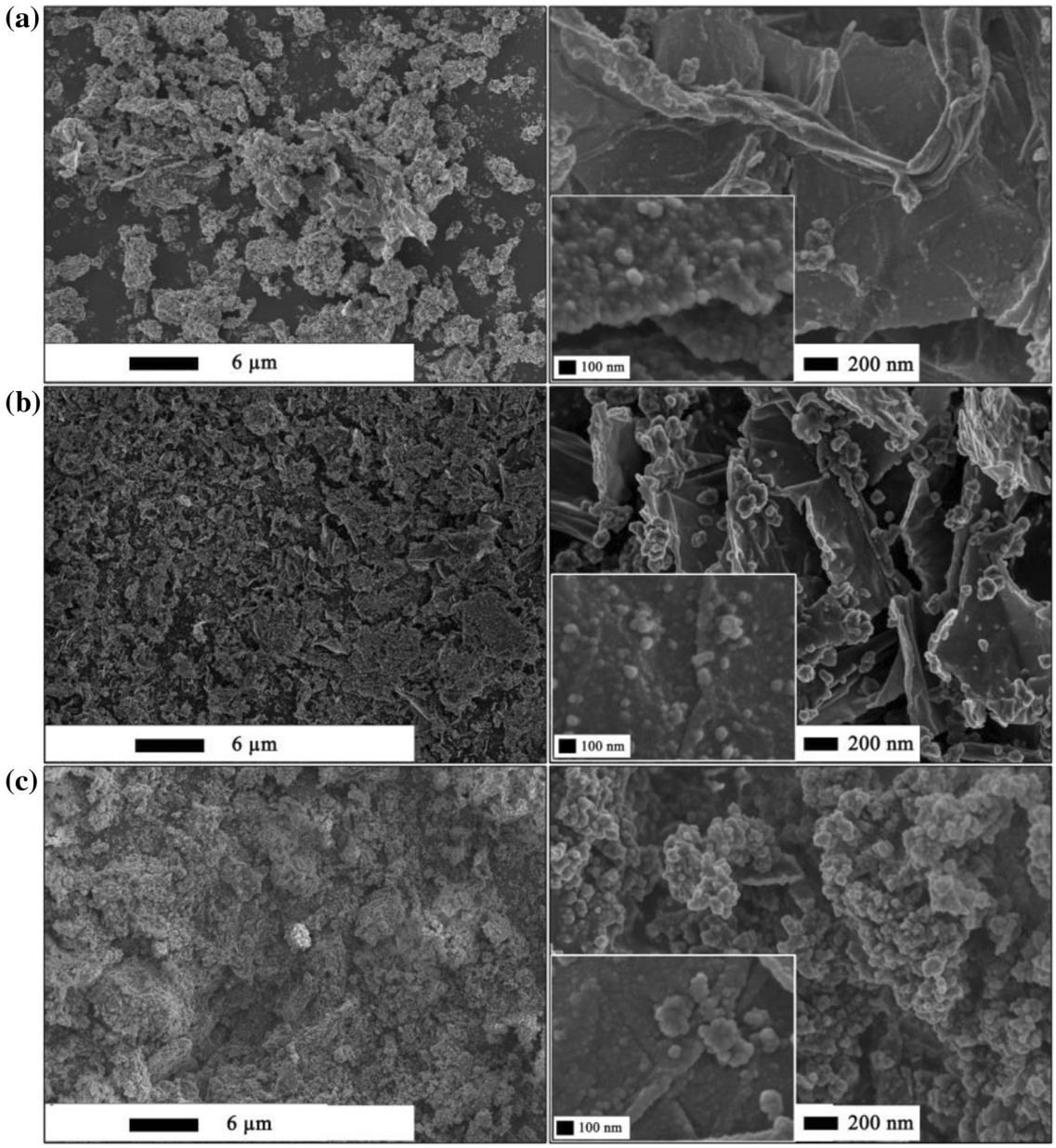

Fig. 4 SEM images obtained for the RGO(5 wt%)/Al_2O_3 nanocomposites thermally decomposed at **a** 0 °C, **b** 280 °C, and **c** 500 °C

magnification images of single RGO flakes. However, the low magnification images revealed the undesirable agglomeration of the final product.

The representative SEM–EDS pattern of the RGO/Al_2O_3 nanocomposite with 5 wt% RGO addition is shown in Fig. 8. As can be observed, EDS analysis taken from the surface of an RGO flake with deposited Al_2O_3 nanoparticles (sharp-marked point) displayed strong C, O, and S peaks next to Al and Na peaks. It should be noted that the existence of S and Na peaks corresponded to the presence of impurities in GO (as a result of using the specific reagents in the modified Hummer's method). The quantitative results of the EDS analysis are presented in Table 1. They reveal the presence of large amounts of carbon (over 80 wt%) and oxygen (ca. 16 wt%) together with a very low amount of aluminium (below 1 wt%). It should, however, be noted that the coverage of the RGO surface by Al_2O_3 nanoparticles is generally not uniform and the amount of single nanoparticles on the surface and edges of RGO flakes is different. The analysis was taken from the point specifically chosen to be relative to the uniform coverage of the RGO surface. Thus, the obtained results indicate that the amount of Al_2O_3 nanoparticles that are able to create the uniform layer on the surface of RGO flakes is de facto not very high.

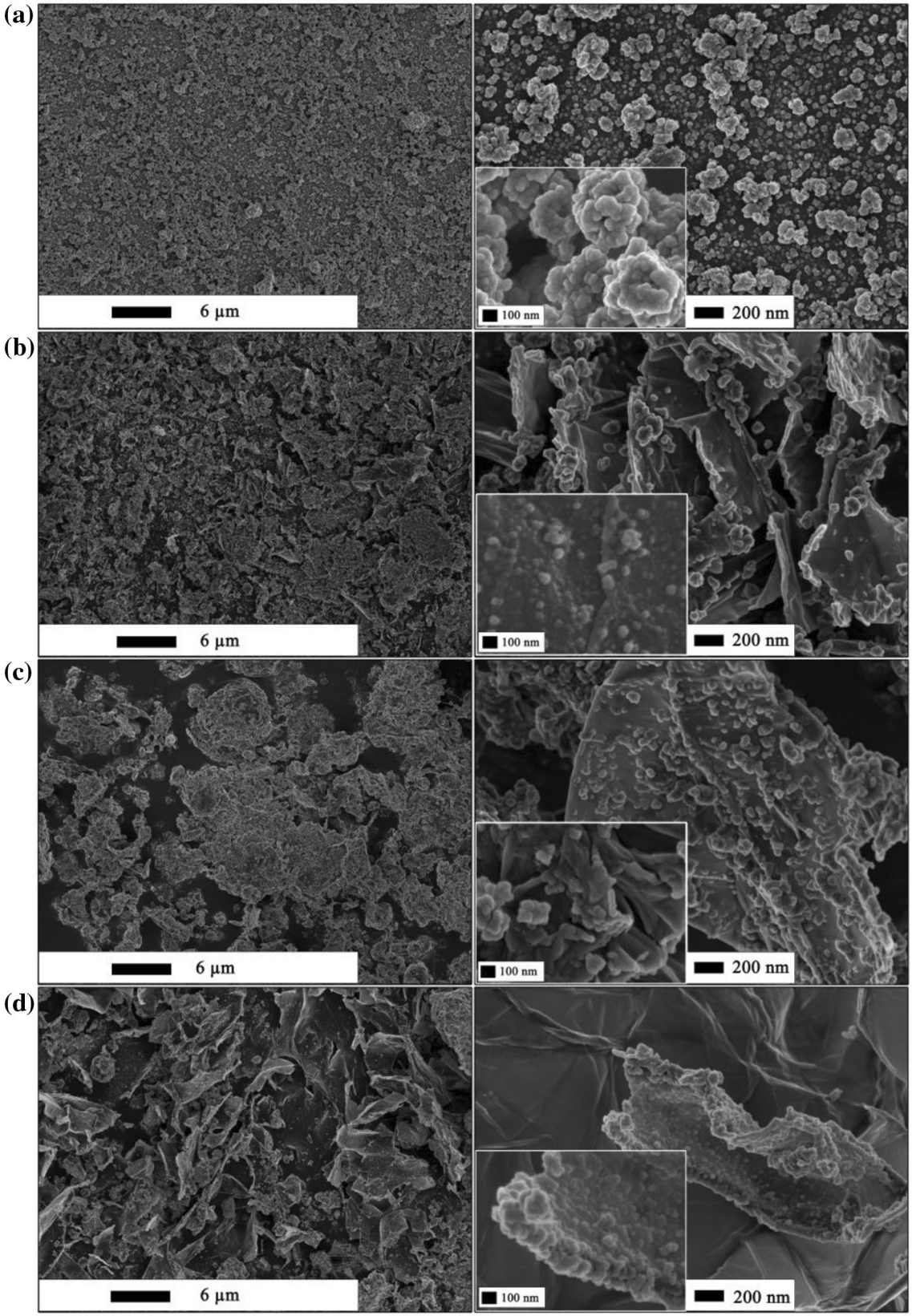

Fig. 5 SEM images obtained for the RGO/Al_2O_3 nanocomposites with **a** 0 wt%, **b** 5 wt%, **c** 10 wt%, and **d** 15 wt% RGO addition. The samples were thermally decomposed at 280 °C

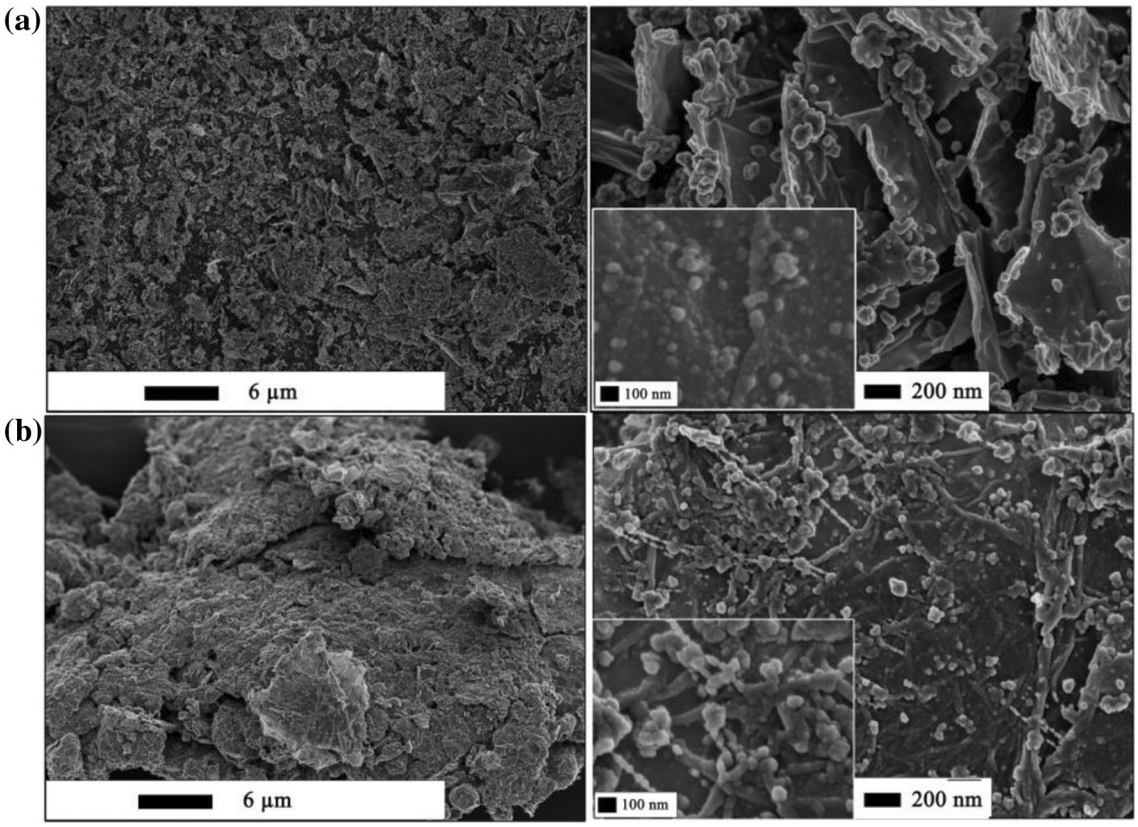

Fig. 6 SEM images obtained for the RGO/Al_2O_3(5 wt%) nanocomposite modified with **a** 0 ml and **b** 0.006 ml Et_2O

The microscopic examinations were also aimed at quantitatively characterizing the morphology of Al_2O_3 nanoparticles embedded on the surface of RGO flakes as well as making a comparison with the Al_2O_3 nanopowder using a statistical (stereological) analysis. The quantitative analysis was performed on the RGO/Al_2O_3(5 wt%) nanocomposite obtained in the R4 process, since it was the most efficient way to prepare the nanocomposite with the best morphology. The results of the particle size analysis are shown in Fig. 9a and in Table 2. As can be seen in Table 2, there were no changes in the shape of Al_2O_3 nanoparticles deposited on the surface of RGO flakes and free Al_2O_3 nanoparticles. The coefficients of shape were close to 1. However, a high reduction of the average value of particle size (d_2) was obtained for Al_2O_3 nanoparticles when deposited on the surface of RGO flakes. The sizes of Al_2O_3 particles deposited on RGO ranged from ca. 20 to 140 nm (the average value being 58 nm) and were lower in comparison with free Al_2O_3 nanoparticles, characterized by sizes ranging from ca. 20 to 180 nm (the average value being 95 nm). It should also be noted that free Al_2O_3 nanoparticles had a high agglomeration tendency. The average agglomerate size measured for Al_2O_3 nanopowder was over 0.3 µm (Fig. 9c) with a relatively low value of the coefficient of variation (0.14) (Table 3).

Physical properties

The results of the investigations of the physical properties of GO and the obtained RGO are presented in Table 4, which shows the values of the specific surface area, S_{BET}, the total pore volume, V_{BJH}, and the average pore diameter, D_{BJH}, of the analysed samples. As expected, the specific surface area of RGO flakes was 1.2 times higher in comparison to GO flakes (Table 4). It is accepted that the presence of chemisorbed water and surface oxygen species generally decreases the surface area measured by physical nitrogen sorption. Thus, our results of increase in the RGO flake BET surface area confirmed that the thermal treatment of GO resulted in the removal of oxygen-containing species from the surface of GO flakes. The specific surface area of Al_2O_3 nanopowder was much lower (53 m^2/g) in comparison with materials containing graphene. GO and RGO flakes were characterized by similar values of total pore volume, which exceeded 0.1 cm^3/g. It should be noted that the pore volume of the RGO/Al_2O_3 (5 wt%) nanocomposite, obtained in the R4 process, was very high (ca. 0.7 cm^3/g) in comparison with other samples.

The nitrogen sorption isotherms obtained for the analysed samples are presented in Fig. 10. The obtained results are in good agreement with the SEM investigation results. They indicate that the shape of the isotherm obtained for

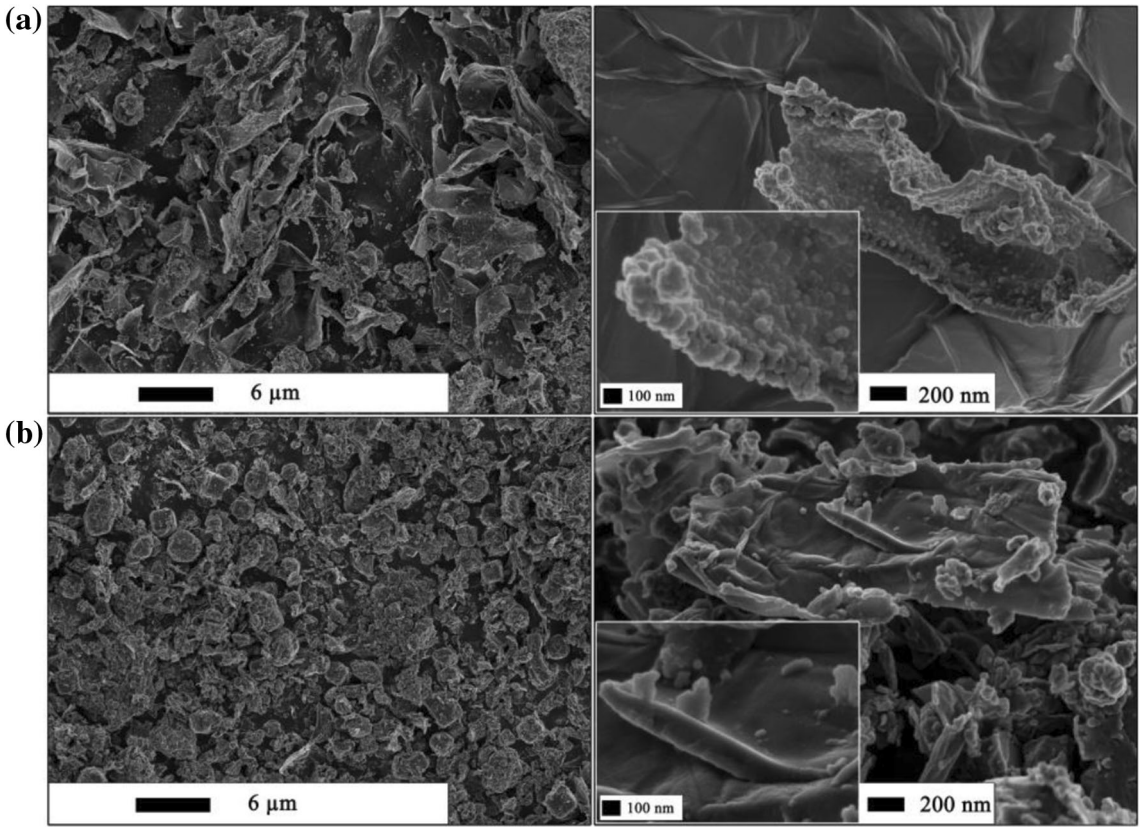

Fig. 7 SEM images obtained for the RGO/Al_2O_3(15 wt%) nanocomposite modified with **a** 0 and 0.01 ml Et_2O

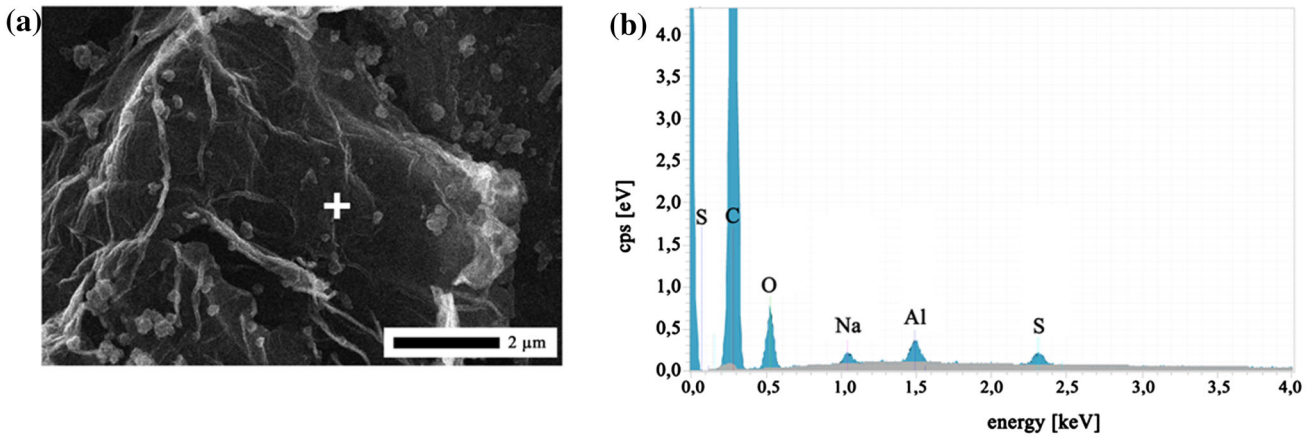

Fig. 8 SEM image of **a** the RGO/Al_2O_3(5 wt%) nanocomposite and **b** the EDS analysis taken from the sharp-marked point of the analysed sample

RGO and GO flakes was typical for graphenes, characterized by the presence of slit-shaped pores (Srinivas et al. 2010). For the RGO/Al_2O_3 nanocomposite, the shape of the isotherm suggested the presence of bottle-shaped pores. It was hard to compare the shape of the isotherm obtained for pure Al_2O_3 due to the very low N_2 adsorption; however; it is already accepted that the shape of the pores of Al_2O_3 is generally spherical or/and bottled (Qadeer and Ikram 2005). Taking into consideration that N_2 particles only adsorb on available surfaces, it can be concluded that the pores in our RGO/Al_2O_3 nanocomposite originated mainly from Al_2O_3 nanoparticles.

XPS spectroscopy

XPS spectroscopy was used for the analysis of the RGO(5 wt%)/Al_2O_3 nanocomposite synthesized in the R4 process. The XPS analysis showed the quantitative chemical

Table 1 Quantitative results of the EDS analysis of the RGO/Al_2O_3 (5 wt%) nanocomposite

Element present	Series	C [wt%]	C_{error} [wt%]
Carbon	K	82.02	9.78
Oxygen	K	15.77	2.71
Aluminium	K	0.98	0.08
Sulphur	K	0.64	0.06
Sodium	K	0.59	0.08

Table 4 Physical properties of GO and RGO flakes as well as the RGO(5 wt%)/Al_2O_3 nanocomposite powder obtained in the R4 process

Sample name	S_{BET}/m^2g^{-1}	V_{BJH}/cm^3g^{-1}	D_{BJH}/nm
GO flakes	178.1	0.1693	4
RGO flakes	227.8	0.1753	4
RGO(5 wt%)/Al_2O_3	242.4	0.7167	1
Al_2O_3	53.0	0.0100	3

composition in the sample as well as the identification of the chemical state of elements present (Table 5). The C1 s peak located at 285 eV was assigned to the presence of the C–C bonds of graphitic carbon (17 at %). The other C1 s peaks were a result of the presence of –C–OH and O=C–OH oxygen-containing species, also according to other researchers (Yang et al. 2009b). The atomic percentage of –C–OH and O=C–OH bonds in the RGO/Al_2O_3 nanocomposite was ca. 7 and 2 at%, respectively. Comparing our results with the typical amount of oxygen on GO (ca. 50 wt%, Jastrzębska et al. 2016), one can observe a considerable reduction of the amount of oxygen groups and the reduction of GO to RGO as a result of the reaction process with triethylaluminium. The Al2p peaks at 74.4 eV (25.21 at %) and the O1 s peaks at 531.2 eV (17.24 at %) and 532.6 eV (21.58 at %) were assigned to the presence of crystalline Al_2O_3 on the surface of RGO. It should be noted that the presence of the crystalline phase of Al_2O_3 was a result of the thermal treatment of the obtained organic precursor. The XPS spectra also revealed the presence of carbonate (CO_3^{2-}) species, in the corresponding O1s peak and C1s peak located at 290.8 and 529.4 eV, respectively. The obtained results thus suggest that the thermal decomposition was an incomplete process, and some amount of the organic precursor remained in the final product. This is justified by taking into

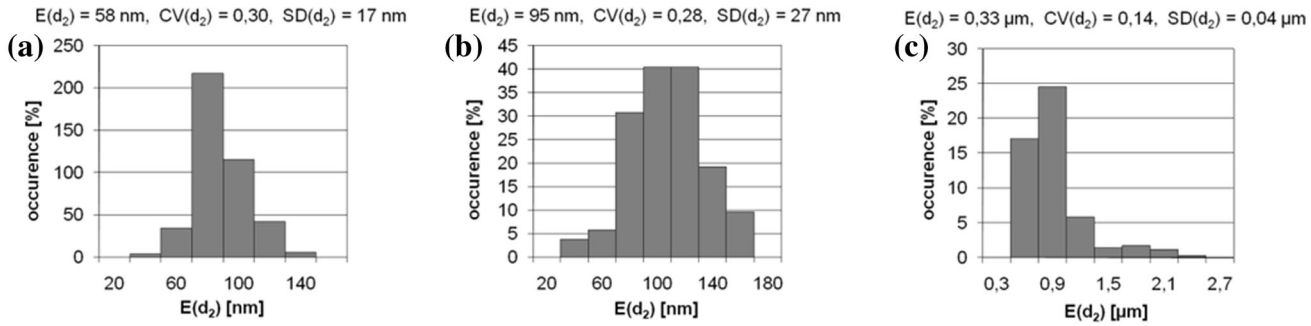

Fig. 9 The distribution of the Al_2O_3 particles size deposited **a** on the surface of RGO flakes as well as **b** on free Al_2O_3 nanoparticles and **c** on agglomerates of the Al_2O_3 nanopowder comparative sample obtained in the R4 process

Table 2 Results of the particle stereological analysis obtained for Al_2O_3 particles deposited on the surface of RGO flakes and free Al_2O_3 particles of the Al_2O_3 nanopowder comparative sample obtained in the R4 process

Sample name	n	Parameter	d_2 (nm)	d_{min} (nm)	d_{max} (nm)	p (nm)	pC (nm)	d_{max}/d_2	d_{min}/d_2	p/pC	$p/(\pi \cdot d_2)$
RGO/Al_2O_3	218	$\bar{x}$	58	53	69	204	197	1.2	0.9	1.0	1.1
		CV(x)	0.30	0.33	0.27	0.27	0.27	0.31	0.14	0.01	0.18
Al_2O_3	78	$\bar{x}$	95	86	114	336	322	1.2	0.9	1.0	1.1
		CV(x)	0.28	0.30	0.27	0.27	0.26	0.30	0.14	0.02	0.17

Table 3 Results of the agglomerate stereological analysis obtained for the Al_2O_3 nanopowder comparative sample obtained in the R4 process

Sample name	n	Parameter	d_2 (nm)	d_{min} (nm)	d_{max} (nm)	p (nm)	pC (nm)	d_{max}/d_2	d_{min}/d_2	p/pC	$p/(\pi \cdot d_2)$
Al_2O_3	188	$\bar{x}$	0.33	0.28	0.37	1.09	1.06	1.12	0.84	1.03	1.06
		CV (x)	0.14	0.15	0.23	0.17	0.17	0.23	0.08	0.01	0.14

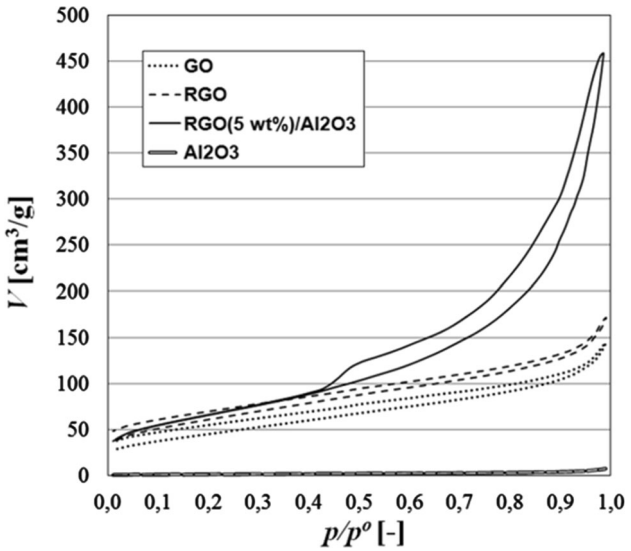

Fig. 10 Nitrogen sorption isotherms obtained for GO and RGO flakes, the RGO(5 wt%)/Al_2O_3 nanocomposite, as well as free Al_2O_3 particles

consideration that the temperature of 280 °C may not be enough for an aluminium triethoxide to fully decompose to aluminium oxide. However, it should be noted that the amount of these species was not considerably high, 1.10 and 3.40 at %, respectively.

Discussion on reactions

We also studied the reactions that may occur at the interface between GO and triethyl aluminium, Et_3Al (or $(C_2H_5)_3Al$) on basis of the obtained results. The sol–gel reactions that occurred during RGO/Al_2O_3 nanocomposite synthesis are represented by the following formulae:

$$\mathrm{RGO} + (\mathrm{C_2H_5})_3\mathrm{Al} \xrightarrow{\mathrm{O_2,\ C_6H_{14}}} (\mathrm{C_2H_5-O})_2\mathrm{Al} - \mathrm{O} - \mathrm{GR} + \mathrm{C_2H_5OH} \quad (1)$$

$$(\mathrm{C_2H_5-O})_2\mathrm{Al} - \mathrm{O} - \mathrm{GR} \xrightarrow{\mathrm{H_2O,\ drying}} (\mathrm{C_2H_5})_2\mathrm{AlOH} - \mathrm{GR} \quad (2)$$

$$(\mathrm{C_2H_5-O})_2\mathrm{Al} - \mathrm{O} - \mathrm{GR} \xrightarrow{\mathrm{H_2O,\ drying}} (\mathrm{C_2H_5})_2\mathrm{Al} - \mathrm{O} - \mathrm{Al}(\mathrm{C_2H_5})_2 \quad (3)$$

$$(\mathrm{C_2H_5-O})_2\mathrm{Al} - \mathrm{O} - \mathrm{GR} \xrightarrow{\mathrm{H_2O,\ drying}} \mathrm{C_2H_5Al} - \mathrm{O} \quad (4)$$

$$(\mathrm{C_2H_5})_2\mathrm{AlOH} - \mathrm{GR} + (\mathrm{C_2H_5})_2\mathrm{Al} - \mathrm{O} - \mathrm{Al}(\mathrm{C_2H_5})_2 - \mathrm{GR} + \mathrm{C_2H_5} - \mathrm{Al} - \mathrm{O} - \mathrm{GR} \xrightarrow{\mathrm{O_2,\ 280\,^\circ C,\ 3\,h}} \mathrm{Al_2O_3} - \mathrm{GR} + \mathrm{CO_2}\uparrow + \mathrm{H_2O}\uparrow + \mathrm{C} \quad (5)$$

The detailed reaction sequences are presented in Fig. 11. In the scheme of the reaction sequence A, an influence of water is exhibited, while the reaction sequence B presents reactions with atmospheric dioxygen. It should be noted that all of the reactions that may occur are already known in the subject literature. According to Ziemkowska and co-workers (Ziemkowska et al. 2014), aluminium trialkyls undergo oxidation, hydrolysis, or both oxidation and hydrolysis depending on the time of triethyl aluminium exposure to air. When H_2O and O_2 are present deficiently in the reaction, Al_2O_3 nanoparticles should be formed and a mild hydrolysis–oxidation-association process should occur because the reaction mixture is just exposed to air (like in the R4 process).

During the production of RGO/Al_2O_3 nanocomposite, Et_3Al was added in an excess to the number of functional groups containing oxygen atoms and bonded to the surface of RGO. According to the literature data (Pasynkiewicz et al. 1977; Bolesławski et al. 1983a, b; Storre et al. 1996; Mason et al. 1993), the first step of an interaction of Et_3Al with these functional groups is a formation of unstable co-ordinate complexes (product A, Fig. 2) with coordinate bonds of Al←OH. The complexes undergo a further reaction with an evolution of ethane and $OAlEt_2$ moieties formation (product B). Only the complex of Et_3Al with the epoxide oxygen is stable. The reaction of the product B with water originating from moisture is the next step, in which ethyl groups bonded to aluminium atoms are gradually removed and substituted by OH groups. Et_3Al molecules coordinated to the epoxide oxygens can be

Table 5 The chemical state of elements present in the RGO(5 wt%)/Al_2O_3 nanocomposite obtained in the R4 process

Signal indication	Peak (eV)	Composition (at. %)	Bond
C1s	285.0	16.53	C–C (graphene)
C1s	287.4	6.67	–C–OH (graphene)
C1s	289.3	1.52	O=C–OH (graphene)
C1s	290.8	1.10	Carbonate (CO_3^{2-})
O1s	529.4	3.40	Carbonate (CO_3^{2-})
O1s	532.6	21.58	Al–O (Al_2O_3)
O1s	531.2	17.24	Al–O (Al_2O_3)
Al2p	74.4	25.21	Al–O(Al_2O_3)

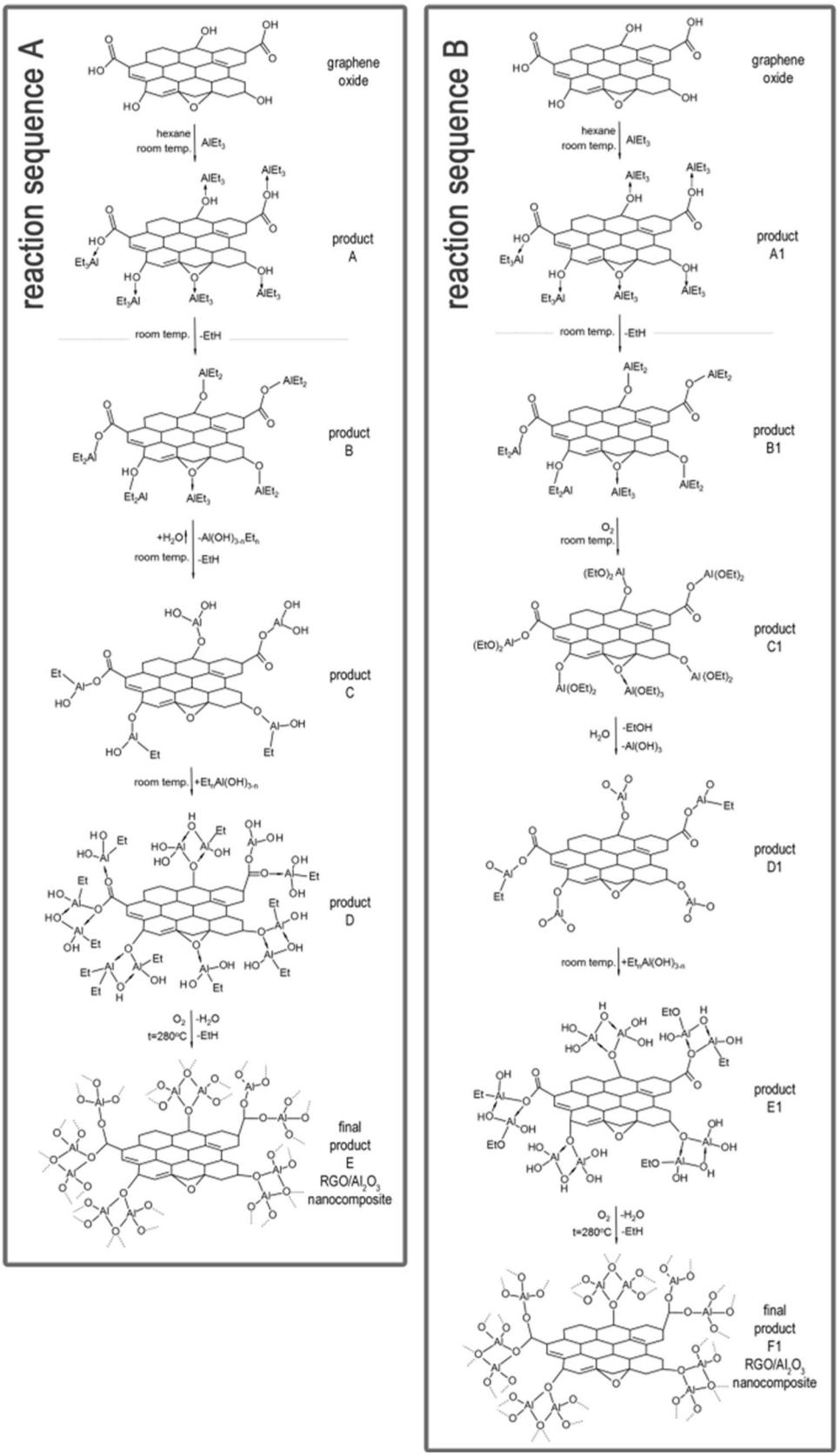

Fig. 11 Scheme describing probable sol–gel reactions (divided into the two sequences) occurring during the RGO/Al_2O_3 nanocomposite synthesis using the R4 process. The 'Et' symbol represents the ethyl (C_2H_5) group

eliminated in the form of ethylhydroxy aluminium $Al(OH)_{3-n}Et_n$. In the obtained product C, the tri-coordinate aluminium atoms have a tendency to increase their coordination number by association with $Al(OH)_{3-n}Et_n$ molecules, mainly formed in the reaction of free Et_3Al with moisture.

As a result of an interaction of $Al(OH)_{3-n}Et_n$ with tri-coordinate aluminium atoms, four-membered Al_2O_2 cycles are formed that are typical for aluminium alkoxides and hydroxides. The thus obtained product D is finally subjected to thermal treatment to remove water and organic moieties in the form of alkanes. The final RGO/Al_2O_3 nanocomposite contains aluminium oxide bonded to the surface of RGO.

Dioxygen present in the air has also an influence on RGO/Al_2O_3 nanocomposite formation (pathway B). According to the literature data (Barron 1993; Lewiński et al. 1996, 1999, 2000), an oxidation of aluminium alkyls leads to a mixture of aluminium alkoxides. In the product B1 (Fig. 11), an interaction of dioxygen with ethyl groups bonded to aluminium atoms results in the transformation of EtAl groups into EtOAl moieties and the formation of the product C1. The product C1 has a chance to react with water to eliminate ethanol and aluminium hydroxide and yield the product D1. After association with $Al(OH)_{3-n}Et_n$ molecules present in the solution yielding the product D1 is transformed into E1 containing tetra-coordinate aluminium atoms. Similarly to the reaction sequence A, the final step of the RGO/Al_2O_3 nanocomposite production is thermal treatment of the precursor. Because there is an excess of triethyl aluminium in solution, extra molecules of Et_3Al and $Al(OH)_{3-n}Et_n$ associate with the EtAl AlOH and AOEt groups bonded with RGO. Therefore, after thermal decomposition of precursors (products D and E1), much more than one aluminium atom per a functional hydroxyl, carboxyl or epoxide group is present in the nanocomposite. These aluminium atoms together with oxygen atoms form a network chemically bonded to the surface of RGO.

Conclusions

The present paper gives new insight into the problem of controlling the morphology of reduced graphene oxide/alumina (RGO/Al_2O_3) nanocomposites. The dry and simplified sol–gel methods of RGO/Al_2O_3 nanocomposite synthesis were compared and the influence of six key synthesis parameters on the morphology of the resulting nanocomposite powders was investigated to optimize the morphology of RGO/Al_2O_3 nanocomposites in terms of reducing the undesired agglomeration of RGO/Al_2O_3 nanocomposite flakes to a significant minority and obtaining the uniform coverage of the RGO surface with Al_2O_3 nanoparticles. Our investigations confirmed that the synthesis parameters have a major influence on the morphology of the investigated RGO/Al_2O_3 nanocomposites. The obtained results indicate that the aluminium triisopropoxide, Al(*i*-PrO)$_3$, makes it possible to obtain a more uniform morphology of the RGO/Al_2O_3 nanocomposite in comparison with triethylaluminium, Et_3Al. It is also better to use hexane as the reaction environment and GO as a substrate for Al_2O_3 deposition in contrast to isopropanol (*i*-PrOH) and RGO, respectively. Diethyl ether used as a modifying agent enabled better and more uniform coverage of GO flakes but also resulted in the undesirable agglomeration of the final product. Also, despite a high excess of Al_2O_3 used (95 wt%), the lowest RGO/Al_2O_3 flake agglomeration and the formation of an uniform layer composed of Al_2O_3 nanoparticles were obtained only when 5 wt% of GO was used in the process. The optimal temperature for thermal decomposition was 280 °C for 3 h under an air atmosphere. The optimal method for RGO/Al_2O_3 nanocomposite synthesis was the R4 process. The nanocomposite thus obtained was characterized by the average size of surface Al_2O_3 particles of 58 nm, the BET-specific surface area of 242.4 m^2/g, and open porosity of 0.7 cm^3/g.

Our results indicate that the optimization of the synthesis process enabled the reduction of the undesired agglomeration of the final product to an insignificant minority. The average size of the Al_2O_3 nanoparticles deposited on the surface of RGO was reduced by ca. 50% in comparison with free Al_2O_3 nanoparticles. Our results also show that during other reaction pathways Al_2O_3 nanoparticles cover RGO flakes non-uniformly. As expected, thermal treatment stimulated the growth and agglomeration of Al_2O_3 nanoparticles deposited on the edges of RGO flakes, which cannot be generally avoided but can be controlled and reduced to an insignificant minority.

This is also the first study with a detailed discussion of reactions expected to occur during the synthesis of the RGO/Al_2O_3 nanocomposite. It is widely accepted that the functional groups present on the surface of GO, including carboxylic, hydroxyl, carbonyl, and epoxy groups, can be utilized as nucleating sites to control the size, morphology, and crystallinity of the nanoparticles grown. Our results show that triethyl aluminium undergoes oxidation and hydrolysis at the same time to yield an organic precursor. When H_2O and O_2 are present deficiently in the reaction only due to the exposure of the reaction mixture to air (like in the R4 process), the mild hydrolysis–oxidation-association process occurs. Because there is an excess of triethyl aluminium in the reaction, association also occurs but without the creation of cage-complexes due to no excess of water.

Acknowledgements The study was accomplished thanks to the funds allotted by the National Science Centre on basis of decision no. DEC-

2013/09/D/ST8/04001, within the framework of the research Project No. UMO-2013/09/D/ST8/04001.

References

Barron AR (1993) Reactions of Group 13 alkyls with dioxygen and elemental chalcogens: from carelessness to chemistry. Chem Soc Rev 22:93–99. doi:10.1039/CS9932200093

Becerril HA, Man J, Liu Z, Stoltenberg RM, Bao Z, Chen Y (2008) Evaluation of solution-processed reduced graphene oxide films as transparent conductors. ACS Nano 2(3):463–470. doi:10.1021/nn700375n

Bolesławski M, Serwatowski J (1983a) Synthesis and structure of alkylaluminoxanes. J Organomet Chem 254:159–166. doi:10.1016/S0022-328X(00)99102-2

Bolesławski M, Serwatowski J (1983b) Investigations of the hydrolysis reaction mechanism of organoaluminium compounds. ^{1}H NMR spectroscopic studies on the R_3Al/H_2O reaction in polar solvents. J Organomet Chem 255:269–278. doi:10.1016/S0022-328X(00)99318-5

Erickson K, Erni R, Lee Z, Alem N, Gannett W, Zettl A (2010) Determination of the local chemical structure of graphene oxide and reduced graphene oxide. Adv Mater 22(40):4467–4472. doi:10.1002/adma.201000732

Fan X, Peng W, Li Y, Li X, Wang S, Zhang G (2008) Deoxygenation of exfoliated graphite oxide under alkaline conditions: a green route to graphene preparation. Adv Mater 20(23):4490–4493. doi:10.1002/adma.200801306

Jastrzębska AM, Kunicki AR, Olszyna AR, Karwowska E (2011a) Al_2O_3–Ag nanopowders: new method of synthesis, characterization and biocidal activity. Adv Appl Ceram 110(2):108–113. doi:10.1179/1743676110Y.0000000014

Jastrzębska AM, Radziun E, Rosłon M, Kunicki AR, Olszyna AR, Dudkiewicz-Wilczyńska J, Anuszewska E, Karwowska E (2011b) In vitro assessment of antibacterial properties and cytotoxicity of Al_2O_3-Ag nanopowders. Adv Appl Ceram 110(6):353–359. doi:10.1179/1743676111Y.0000000023

Jastrzębska AM, Kunicki AR, Olszyna AR (2011c) Study of the properties of Al_2O_3–Ag nanopowders produced by an innovative thermal decomposition-reduction and silver nitrate reduction methods. Key Eng Mater 478:13–18. doi:10.4028/www.scientific.net/KEM.478.13

Jastrzębska AM, Kurtycz P, Olszyna AR (2012) Recent advances in graphene family materials toxicity investigations. J Nanopart Res 14(1320):1–21. doi:10.1007/s11051-012-1320-8

Jastrzębska AM, Karwowska E, Tabernacka A, Mosdorf P, Polis P, Kurtycz P, Olszyna A, Kunicki AR (2013) New non phyto- and eco-toxic alumina-stabilized silver and praseodymium nanoparticles. Int J Appl Ceram Technol 10(6):908–916. doi:10.1111/j.1744-7402.2012.02834.x

Jastrzębska AM, Kurtycz P, Olszyna AR, Jureczko J, Kunicki AR (2014) New alumina-based novel ceramic nanopigments: an alternative to the purple of cassius. Int J Appl Ceram Technol 11(4):738–744. doi:10.1111/ijac.12099

Jastrzębska AM, Jureczko J, Kunicki AR, Olszyna AR (2015a) New reduced graphene oxide/alumina (RGO/Al_2O_3) nanocomposite: innovative method of synthesis and characterization. Int J Appl Ceram Technol 12(3):522–528. doi:10.1111/ijac.12183

Jastrzębska AM, Karwowska E, Olszyna AR, Kunicki A (2015b) Influence of bacteria adsorption on zeta potential of Al_2O_3 and Al_2O_3/Ag nanoparticles in electrolyte and drinking water environment studied by means of zeta potential. Surf Coat Technol 271:225–233. doi:10.1016/j.surfcoat.2014.12.015

Jastrzębska AM, Karcz J, Letmanowski R, Zabost D, Ciecierska E, Zdunek J, Karwowska E, Siekierski M, Olszyna A, Kunicki A (2016) Synthesis of the RGO/Al_2O_3 core-shell nanocomposite flakes and characterization of their unique electrostatic properties using zeta potential measurements. Appl Surf Sci 362:577–594. doi:10.1016/j.apsusc.2015.10.125

Jiang G, Lin Z, Chen C, Zhu L, Chang Q, Wang N, Wei W, Tang H (2011) TiO2 nanoparticles assembled on graphene oxide nanosheets with high photocatalytic activity for removal of pollutants. Carbon 49(8):2693–2701. doi:10.1016/j.carbon.2011.02.059

Jusza A, Anders K, Jastrzębska A, Polis P, Olszyna A, Kuś M, Kunicki A, Piramidowicz R (2011) Luminescent and structural properties of $Yb3^{+}$-doped Al2O3 nanopowders. Opt Mater 33(10):1487–1491. doi:10.1016/j.optmat.2011.04.015

Karwowska E, Mrozowicz M, Zawada A, Ząbkowski T, Ziemkowska W, Kunicki AR, Olszyna A (2002) Impact of Al_2O_3 nanopowders characterised by various hysicochemical properties on growth of green alga Scendesmus quadricauda. Adv Appl Ceram 111:142–148. doi:10.1179/1743676111Y.0000000062

Lewiński J, Zachara J, Grabska E (1996) Synthesis and molecular structure of $(^{t}BuOO)(^{t}BuO)Al(\mu\text{-}O^{t}Bu)^{2}Al(mesal)^{2}$. The first structurally characterized (alkylperoxo)aluminum compound. J Am Chem Soc 118:6794–6795. doi:10.1021/ja961083f

Lewiński J, Zachara J, Kopeć T, Madura I, Prowotorow I (1999) On the mechanism of four-coordinate aluminum alkyls interaction with dioxygen: evidence for spatial demands in the autoxidation reaction. Inorg Chem Commun 2:131–134. doi:10.1016/S1387-7003(99)00029-5

Lewiński J, Zachara J, Goś P, Grabska E, Kopeć T, Madura I, Marciniak W, Prowotorow I (2000) Reactivity of various four-coordinate aluminum alkyls towards dioxygen: evidence for spatial requirements in the insertion of an oxygen molecule into the Al–C bond. Chem A Eur J 6:3215–3227. doi:10.1002/1521-3765(20000901)6:17<3215:AID-CHEM3215>3.0.CO;2-8

Li Y, Zhang P, Du Q, Peng X, Liu T, Wang Z, Xia Y, Zhang W, Wang K, Zhu H, Wu D (2011) Adsorption of fluoride from aqueous solution by graphene. J Colloid Interface Sci 363(1):348–354. doi:10.1016/j.jcis.2011.07.032

Liang Y, Wang H, Sanchez Casalongue H, Chen Z, Dai H (2010) TiO2 nanocrystals grown on graphene as advanced photocatalytic hybrid materials. Nano Res 3(10):701–705. doi:10.1007/s12274-010-0033-5

Mason MR, Smith JM, Bott SG, Barron AR (1993) Hydrolysis of tri-tert-butylaluminum: the first structural characterization of alkylalumoxanes $[(R_2Al)_2O]n$ and $(RAlO)_n$. J Am Chem Soc 115:4971–4984. doi:10.1021/ja00065a005

Mattevi C, Eda G, Agnoli S, Miller S, Mkhoyan KA, Celik O (2009) Evolution of electrical, chemical and structural properties of transparent and conducting chemically derived graphene thin films. Adv Funct Mater 19(16):2577–2583. doi:10.1002/adfm.200900166

Mavarro CG, Meyer JC, Sundaram RS, Chuvilin A, Kurasch S, Burghard M (2010) Atomic structure of reduced graphene oxide. Nano Lett 10(4):1144–1148. doi:10.1021/nl9031617

Neto C, Guinea AF, Peres NM, Novoselov KSS, Geim AK (2009) The electronic properties of graphene. Rev Mod Phys 81(1):109–162. doi:10.1103/RevModPhys.81.109

Novoselov KS, Geim AK, Morozov SV, Jiang D, Zhang Y, Dubonos SV (2004) Electric field effect in atomically thin carbon films. Science 306(22):666–669. doi:10.1126/science.1102896

Pasynkiewicz S, Sadownik A, Kunicki A (1977) Proton magnetic resonance evidence for the dimethylaluminium hydroxide. J Organomet Chem 124:265–269. doi:10.1016/S0022-328X(00)92590-7

Peter A, Mihaly-Cozmuta L, Mihaly-Cozmuta A, Nicula C, Jastrzębska A, Kurtycz P, Olszyna A (2015) Morphology, structure, and photoactivity of two types of graphene oxide–TiO_2 composites. Chem Pap 69(6):839–855. doi:10.1515/chempap-2015-0088

Polis P, Mosdorf P, Karwowska E, Jastrzebska A, Olszyna A, Kunicki A, Piramidowicz R, Anders K, Jusza A (2013) Influence of Al2O3/Pr nanoparticles on soil, air and water microorganisms. Adv Struct Mater 29:1–8. doi:10.1007/978-3-642-31470-4_1

Qadeer R, Ikram S (2005) Cobalt impregnated alumina: nitrogen adsorption study at 77 K. Turk J Chem 29:101–106

Shin HJ, Kim KK, Benayad A, Yoon SM, Park HK, Jung IS (2009) Efficient reduction of graphite oxide by sodium borohydride and its effect on electrical conductance. Adv Funct Mater 19(12):1987–1992. doi:10.1002/adfm.200900167

Singh V, Joung D, Zhai L, Das S, Khondaker SI, Seal S (2011) Graphene based materials: past, present and future. Prog Mater Sci 56:1178–1271. doi:10.1016/j.pmatsci.2011.03.003

Srinivas G, Zhu Y, Piner R, Skipper N, Ellerby M, Ruoff R (2010) Synthesis of graphene-like nanosheets and their hydrogen adsorption capacity. Carbon 48:630–635. doi:10.1016/j.carbon.2009.10.003

Stankovich S, Dikin DA, Piner RD, Kohlhaas KA, Kleinhammes A, Jia Y (2007) Synthesis of graphene-based nanosheets via chemical reduction of exfoliated graphite oxide. Carbon 45(7):1558–1565. doi:10.1016/j.carbon.2007.02.034

Storre J, Klemp A, Roesky HW, Schmidt H-G, Noltemeyer M, Fleischer R, Stalke D (1996) Hydrolysis of trimesitylgallium and trimesitylaluminum: structures along a reaction pathway. J Am Chem Soc 118:1380–1386. doi:10.1021/ja953213a

Tian J, Liu Y, Tian S, Liu D, Liu C (2015) Fabrication of alumina/graphene composite and its catalytic application property in the selective hydrodesulfurization of fcc gasoline oil. www.paper.edu.cn/en_releasepaper/downPaper/201203-189.html. Accessed 18 Aug 2016

Wang S, Chia PJ, Chua LL, Zhao LH, Png RQ, Sivaramakrishnan S (2008) Band-like transport in surface-functionalized highly solution-processable graphene nanosheets. Adv Mater 20(18):3440–3446. doi:10.1002/adma.200800279

Wang H, Robinson JT, Diankov G, Dai H (2010) Nanocrystal growth on graphene with various degrees of oxidation. J Am Chem Soc 132(10):3270–3271. doi:10.1021/ja100329d

Watcharotone S, Dikin DA, Stankovich S, Piner R, Jung I, Dommett GHB (2007) Graphene–silica composite thin films as transparent conductors. Nano Lett 7(7):1888–1892. doi:10.1021/nl070477+

Wu ZS, Ren W, Gao L, Liu B, Jiang C, Cheng HM (2009) Synthesis of high-quality graphene with a pre-determined number of layers. Carbon 47(2):493–499. doi:10.1016/j.carbon.2008.10.031

Yang D, Velamakanni A, Bozoklu G, Park S, Stoller M, Piner RD, Stankovich S, Jung I, Field DA, Ventrice CA Jr, Ruoff RS (2009a) Chemical analysis of graphene oxide films after heat and chemical treatments by X-ray photoelectron and Micro-Raman spectroscopy. Carbon 47(1):145–152. doi:10.1016/j.carbon.2008.09.045

Yang X, Zhang X, Ma Y, Huang Y, Wang Y, Chen Y (2009b) Superparamagnetic graphene oxide–Fe3O4 nanoparticles hybrid for controlled targeted drug carriers. J Mater Chem 19(18):2710–2714. doi:10.1039/b821416f

Zhang Y, Mo G, Li X, Zhang W, Zhang J, Ye J, Huang X, Yu C (2011) A graphene modified anode to improve the performance of microbial fuel cells. J Power Sources 196(13):5402–5407. doi:10.1016/j.jpowsour.2011.02.067

Ziemkowska W, Basiak D, Kunicki A, Zawada A, Kurtycz P, Olszyna A (2014) Controlled synthesis of alumina using trialkylaluminium as starting materials. Main Group Chem 13(2):105–115. doi:10.3233/MGC-140126